Semiconductor Science and Technology

Performance Enhancement of a Proposed Solar Cell Microstructure Based on Heavily Doped Silicon Wafers

To cite this article before publication: Marwa S Salem *et al* 2019 *Semicond. Sci. Technol.* in press https://doi.org/10.1088/1361-6641/ab0078

Performance Enhancement of a Proposed Solar Cell Microstructure Based on Heavily Doped Silicon Wafers

Marwa. S. Salem[1,2], A. Zekry[3], A. Shaker[4,*], M. Abouelatta[3] and Tarek M. Abdolkader[5]

[1] Department of Electrical Communication and Electronics Systems Engineering, Faculty of Engineering, Modern Science and Arts University, Cairo, Egypt.

[2] Department of Computer Engineering, Computer College, Hail University, Hail, Saudi Arabia.

[3] Department of Electronics and Communications, Faculty of Engineering, Ain Shams University, Cairo, Egypt.

[4] Engineering Physics and Mathematics Department, Faculty of Engineering, Ain Shams University, Cairo, Egypt.

[5] Department of Basic Engineering Sciences, Faculty of Engineering, Benha University, Egypt.

Abstract

This paper aims to present a proposed *npn* solar cell microstructure based on low-cost heavily doped Silicon wafers. The physical perception of the proposed structure is based on the idea of vertical generation and lateral collection of light generated carriers. It should be mentioned that our structure can be utilized whenever the diffusion length of photogenerated electron hole pairs is smaller than the penetration depth of the solar radiation. The enhancement in the structure performance is attained by the optimization of the structure technological and geometrical parameters and based on practical considerations. This enhancement enables achieving the maximum possible structure conversion efficiency. Moreover, the optical performance, in terms of the spectral response and external quantum efficiency, is presented. The optimization is carried out using SILVACO TCAD process and device simulators. The main parameters used in optimization include the thickness and doping of the top n^+ layer as well as the sidewall emitter. Additionally, the structure base width along with the notch depth are considered. Finally, back surface treatment is introduced. The structure conversion efficiency in the initial step before optimization was 10.7%. As a result of the optimization process, the structure conversion efficiency is improved to about 15% above the initial case study by 4%.

Keywords: *npn* solar cell; SILVACO TCAD; heavily doped silicon wafers; conversion efficiency.

* E-mail : ahmed.shaker@eng.asu.edu.eg

1. Introduction

Recent research work devoted to PV systems is directed towards reducing the cost of PV modules. A high percentage of the cost of silicon PV cells comes from the production of the high-quality silicon wafers [1]. Additionally, commercial silicon solar cells require micrometers and even submillimeter thickness to maximize light absorption [2].

To overcome the high cost of PV cells, several attempts have been searched. In this regard, thin-film PV cells have been fabricated from Copper Indium Gallium Sulfide (CIGS), Cadmium Telluride (CdTe), and Gallium Arsenide (GaAs) [3]. These technologies are designed to achieve similar efficiencies to silicon wafer-based PV cells, while using very thin absorber layers. However, they introduce additional issues such as the scarcity (Indium, Gallium) and toxicity (Cadmium, Arsenic) of some elements and the high-cost for fabrication due to deposition systems used. On the other hand, thin-film silicon PV cells fabricated from amorphous silicon suffer from stability problems [4]. Amorphous silicon can be crystallized into polycrystalline silicon grown on low-cost amorphous substrates, however, the quality of such silicon PV cells is still poor [5, 6].

An alternative approach pursued to reduce the cost of c-Si PVs is to significantly reduce the thickness of the Si wafer from the conventional value of 180 μm down to 80 μm, which is considered to be the lower limit regarding practical considerations [7]. Yet, the dramatic reduction in wafer thickness requires the development of light management methods that preserve maximum absorption of solar radiation in spite of reduced thickness.

One of the most promising trends to achieve low cost solar cells is using an inexpensive material such as highly doped silicon wafers. Unfortunately, such inexpensive materials always have high level of impurities or high density of defects. This, in turn, results in low minority carrier's diffusion length [8, 9] and, consequently, diminishes carrier collection and degrades the cell performance. The solution of such a problem could be achieved by generating electron-hole pairs from light absorption vertically and then collecting them laterally. This idea paves the way for using low quality, low cost commercially available highly doped silicon solar cells.

The solar grade silicon production can be extended to produce heavily doped single crystal Si wafers for use as a staring material for our proposed solar cell structure. If one could produce high efficiency solar cells from heavily doped silicon, one can reduce the purification steps of the solar grade silicon and thereby reduce drastically the production cost. So, our investigations on the yield of the heavily doped silicon as a solar cell can lead to an approach to lower the cost of stable

solar cells. In fact, these investigations must be complemented by intensive research on solar grade silicon production techniques. Both can introduce an alternative solution to low cost silicon solar cells.

In this paper, a proposed solar cell structure is explored [10] with a detailed study of the impact of the geometrical and technological parameters on its performance. Each main parameter is varied at a time while keeping the others constant to demonstrate the effect of this parameter solely. Then, the process is repeated for the other parameters. In each optimization step, the conversion efficiency is required to be maximum. Also, the optical performance, in terms of the spectral response and external quantum efficiency, is presented. The optimization is carried out using SILVACO TCAD process and device simulators taking into consideration the practical physical models and their corresponding parameters. Firstly, the thickness and doping of the top n^+ layer, as well as the sidewall emitter, are optimized. After that, the optimization of the structure base width along with the notch depth is explained. Moreover, the optimum structure back surface treatment is introduced. Finally, the dark characteristic of the solar cell is explored. It should be pointed out that our structure can be utilized whenever the diffusion length of photogenerated electron hole pairs is smaller than the penetration depth of the solar radiation.

2. Solar Cell Structure and Parameters

Figure 1(a) presents the *npn* solar cell structure showing its geometrical and technological parameters. The structure is created using SILVACO Athena process simulator [11] as shown in Figure 1(b). Concerning the p^+ base doping, it is chosen to be 10^{18} cm^{-3}. This doping could be attained from a highly-doped starting silicon wafers which are commercially-available wafers. For this doping, the electron diffusion length, L_n, is assumed to be 12 µm [12]. The width W_p must be smaller than L_n, to overcome bulk recombination and increase short circuit current, thus W_p is chosen to be 8 µm. Also, it is important to determine the electron life time. Based on some lifetime measurements [13-16], τ_{no} is chosen to be 5 µsec.

In this study, the sidewalls of the n^+ emitter are passivated with silicon dioxide. This is because the silicon dioxide decreases the gradient of the excess carriers at the structure sidewall surfaces. This means that the passivation decreases the recombination current at sidewall surfaces. Thus, the reverse saturation current decreases and V_{oc} increases.

Regarding the sidewall n^+ emitter parameters, its doping is initially chosen to be high, 5×10^{19} cm^{-3}, to enhance its injection efficiency. At this doping, the hole diffusion length L_p is about 0.5 µm [12]. The bulk recombination is not the major effect regarding the n^+ emitter design because the emitter thickness W_n is narrow with respect to W_p. W_n is chosen to be 0.1 µm. Based on measurements of various emitter types [16], τ_{po} is about 5 µsec at the selected doping level. For the top n^+, its doping and thickness are the same as the lateral emitter. So, its doping is 5×10^{19} cm^{-3} and its thickness is 0.1 µm. Table 1 summarizes the various geometrical and technological parameters for the used case study [10]. The mentioned parameters are going to be used in the simulation of the structure performance for each optimization step unless otherwise stated.

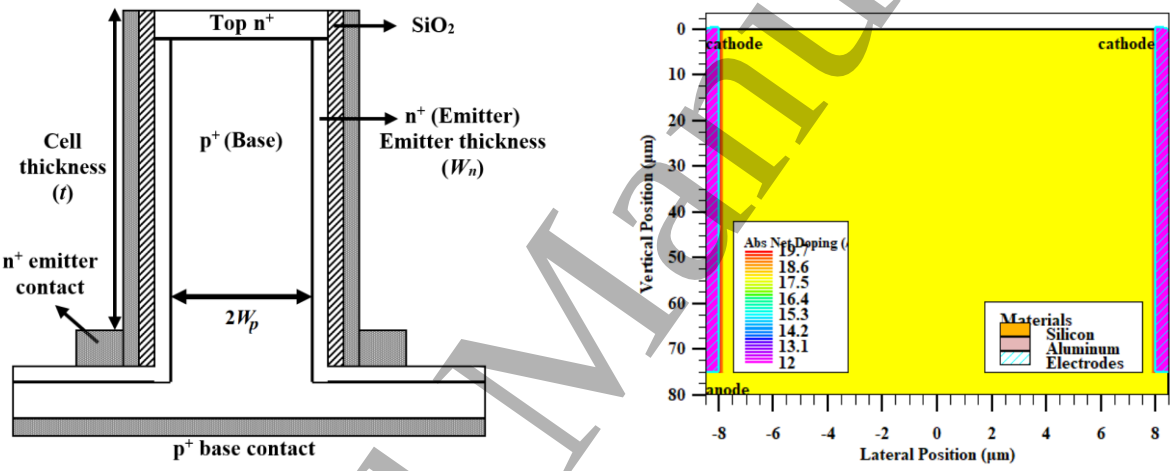

(a) (b)

Figure 1. (a) The *npn* structure parameters for the case study (b) Solar cell structure using SILVACO Athena process simulator.

Table 1 Geometrical and technological parameters of the *npn* structure of a case study.

Structure Parameter	**Value**
Base Width (W_p)	8 µm
Base Doping	10^{18} cm^{-3}
Side Wall Emitter Width (W_n)	0.1 µm
Side Wall Emitter Doping	5×10^{19} cm^{-3}
Device Thickness	80 µm
Top n^+ Layer Thickness	0.1 µm
Top n^+ Layer Doping	5×10^{19} cm^{-3}

3. Results and Discussion

In this section, the impact of variation of *npn* solar cell structure parameters on its performance is studied. These studies are based on enhancing the structure performance by optimizing its parameters. The enhancement concerns both increasing the structure conversion efficiency and reducing its cost. Further, a discussion at the end of this section of the dark characteristics of the cell structure is given to give an overview about the recombination mechanisms encountered within the device. All simulations are carried out by using SILVACO Atlas device simulator [17]

Firstly, the impact of the variation of the top n^+ layer thickness and doping on the performance is studied. In this part, a quantitative comparison between the *npn* with and without top n^+ layer is presented. The objective of this comparison is to prove that the *npn* structure performance with a top n^+ layer is better. This is because the top n^+ layer helps the main sidewall n^+ in enhancing the collection of the input spectrum. After that, the effect of the sidewall n^+ layer, the structure n^+ emitter, on the cell performance is studied. The main concern of this study is to make it a good emitter. Thus, it is designed with the condition that its injection efficiency increases and dark current decreases. The study is carried out from two points of views: doping and width. Furthermore, the effect of the *npn* structure p^+ base width, W_p, on its performance is illustrated. The notch depth is also studied. Finally, the effect of the structure back surface on its performance is considered to be able to reduce the losses caused by the back surface.

A. Effect of the top n^+ layer parameters

The main objective in the design of the top n^+ layer is to be an ultraviolet collector and to give the highest conversion efficiency. Its design considers two important parameters: the first parameter is its thickness which has to be shallow to be able to collect ultraviolet generated carriers, the second parameter is its doping - which must not be too high to prevent the rapid collection of the ultraviolet generated carriers. Thus, it has an optimum value which is to be determined hereinafter.

The ultraviolet part of the solar radiation spectrum contains the highest energetic photons. It is absorbed in a thickness around 0.1 μm [18-21]. Qualitatively, the best thickness of the top n^+ layer to be ultraviolet collector is expected to be 0.1 μm. In the study of the effect of the top n^+

layer thickness on the *npn* structure performance, a comparison between four cases is performed. The first case is when the thickness of top n^+ layer is 0.25 µm. This is the thickness for the conventional planar solar cell [22]. The second case is for a thickness of 0.1 µm. In these cases, the doping of the top n^+ layer is fixed at 5×10^{19} cm^{-3}. The other two cases are without the top n^+ layer. A complete electrical and optical characterization for the four cases is carried out.

Figure 2 shows the *I–V* characteristics for the four studied cases of emitter thickness, 0.1, 0.25 µm, with and without the n^+ layer. From the figure, it is obvious that the *npn* structure without top n^+ layer has the lowest value of I_{sc} and V_{oc}. The reason is that in the absence of the top n^+ layer, it causes the structure to collect only from sidewall junctions. Thus, the structure only collects the long wavelength part of the solar radiation spectrum. Regarding the two other cases, it is obvious that, both I_{sc} and V_{oc} for thickness of 0.1 µm are better than for 0.25 µm. This result is expected, as 0.1 µm thickness collects the ultraviolet part of the spectrum more than the 0.25 µm case.

Table 2 presents all the extracted electrical performance parameters, I_{sc}, V_{oc}, *FF* and η_c, for the four cases. For I_{sc}, its maximum value is at 0.1 µm thickness with a top n^+ layer. This result is expected, as shallower junction collects more from the input spectrum [20, 21]. Concerning I_{sc} for 0.25 µm, it is lower than 0.1 µm for both cases as expected. For the *npn* structure without n^+ layer, it has the lowest I_{sc}.

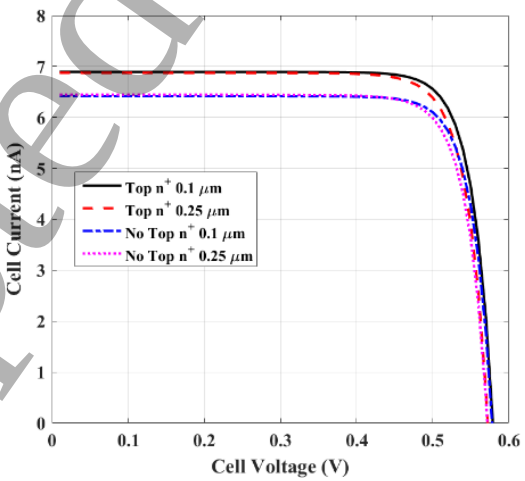

Figure 2. *I–V* characteristics for the four studied cases of the top n^+ layer thickness.

Table 2 Electrical performance parameters of various top n^+ layer thicknesses.

	No top n^+ layer (emitter 0.1 µm)	**No top n^+ layer (emitter 0.25 µm)**	**Top n^+ thickness (0.1 µm)**	**Top n^+ thickness (0.25µm)**
I_{sc} (nA)	6.42	6.46	6.89	6.86
V_{oc} (V)	0.578	0.572	0.579	0.572
***FF* (%)**	82.25	82.04	82.16	81.75
η_c (%)	13.64	13.54	14.66	14.33

A comparison between the optical performance parameters for the four studied cases of the top n^+ layer thickness is also carried out. Firstly, the quantum efficiency of all cases is presented in Figure 3(a). Concerning the *npn* structure without the top n^+ layer, it is obvious that it doesn't collect the ultraviolet part of the spectrum with high efficiency because of the absence of top n^+ layer. Furthermore, Figure 3(b) shows the spectral response. As the spectral response is an indication for I_{sc}, it has the lowest amplitude for the *npn* structure without top n^+ layer.

As a conclusion from the study of the effect of top n^+ layer thickness on the *npn* solar cell structure performance, the best thickness is 0.1 µm. This thickness enables, beside the sidewall emitter, the *npn* structure to collect most of the input spectrum. It gives the highest conversion efficiency, which is the main measure parameter of solar cell performance.

Next, the impact of the top n^+ layer doping, as well as emitter doping is studied. This study is based on two main factors. Firstly, the doping of both top and sidewall n^+ layers must not be too high to prevent the quick recombination of the generated carriers. Secondly, the doping must not be too low to prevent reducing the structure fill factor. When doping decreases, the reverse saturation current increases which results in reducing the fill factor. The open circuit voltage is inversely proportional to the logarithmic of the reverse saturation current. Thus, the fill factor is expected to be affected more than V_{oc} by low doping of the top n^+ layer as explained hereafter in the *I-V* characteristics and electrical performance parameters. As a result, the doping of the top n^+ layer has an optimum value which is going to be determined in this section.

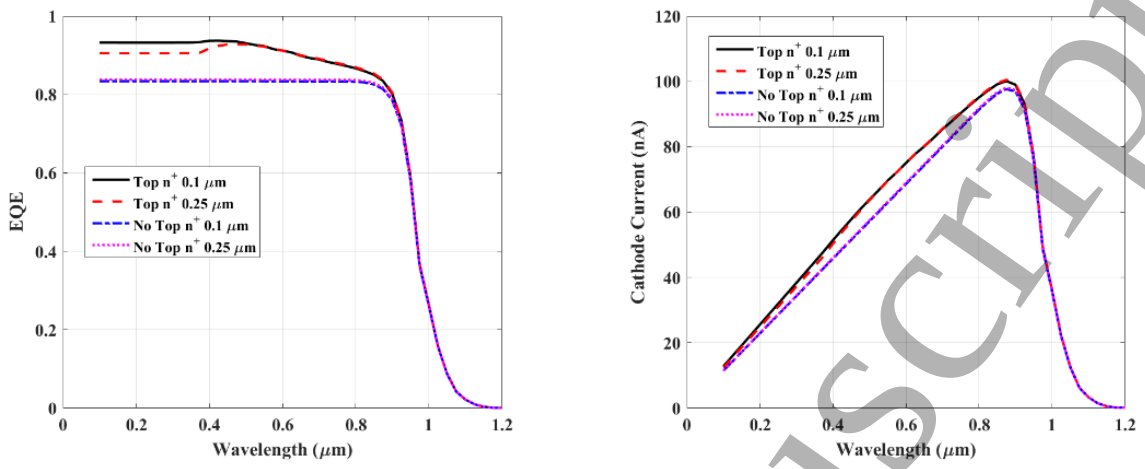

(a) (b)

Figure 3. Impact of the top n^+ layer thickness (a) Quantum and (b) Spectral response.

To study of the impact of the top n^+ layer doping on the *npn* structure performance, a comparison between various values of doping is carried out. The doping values to be studied are ranging from 10^{19} to 10^{20} cm^{-3}. These values contain relatively low doping concentration when talking about the emitter which is 10^{19}, and high doping, 10^{20} cm^{-3}. The thickness of the top n^+ layer here is fixed at 0.1 µm. Practical measured values from wafers for minority carriers' life time with its diffusion lengths [12-16] are used to determine τ_p and L_p at different doping concentrations.

Table 3 shows all the extracted electrical performance parameters for the cases of the top n^+ layer doping. For both I_{sc} and J_{sc}, they are decreased with increasing the doping. The reason is that, by increasing the doping, the recombination of the light generated carriers in the top n^+ layer increases thus the short circuit current and its density decrease. But, this reduction is not severed. The open circuit voltage also decreases following the change in I_{sc}. For the fill factor, it increases with increasing the doping till 3×10^{19} cm^{-3} then it decreases. This is caused by increasing the doping as the reverse saturation current decreases. Regarding the conversion efficiency, it is obvious that the best doping for the top n^+ layer is 2×10^{19} cm^{-3}.

The top n^+ layer thickness and doping enhance the *npn* structure conversion efficiency by 4% compared to the case of the previously published *npn* structure [10]. Thus, the top n^+ layer best thickness is 0.1 µm with doping of 2×10^{19} cm^{-3}. The results reveal that the structure responds and collects most of the input solar radiation spectrum by just adjusting the design of both the thickness

and doping of the top n^+ layer as well as the sidewall emitter. It doesn't need expensive materials with different band gaps as in multi–junction solar cells [23-25].

Table 3: Electrical performance parameters of various top n^+ layer doping.

Doping (cm^{-3})	**10^{19} (τ_{po} = 10 µs)**	**2×10^{19} (τ_{po} = 8 µs)**	**3×10^{19} (τ_{po} = 7 µs)**	**5×10^{19} (τ_{po} = 5 µs)**	**10^{20} (τ_{po} = 1 µs)**
I_{sc} (nA)	6.9	6.9	6.89	6.89	6.85
V_{oc} (V)	0.583	0.583	0.582	0.579	0.563
FF (%)	82.07	82.18	82.22	82.16	81.62
η_c (%)	14.76	14.77	14.75	14.66	14.06

B. Effect of the n^+ Sidewall Emitter parameters

The n^+ sidewall emitter must be designed based on two main parameters: its doping and its width. In this subsection, the effect of variation of the sidewall n^+ emitter width, W_n, on the *npn* structure performance is investigated while the doping of the sidewall n^+ emitter has two values for comparison, 2×10^{19} cm^{-3} (same value as n^+ top layer) and 5×10^{19} cm^{-3}. The best value of W_n must be selected such that it decreases the reverse saturation current. As W_n is very narrow with respect to W_p, its contribution to the illumination in not important.

In table 4, it is seen that the efficiency exhibits a local maximum at emitter width of 0.1 µm. This can be explained as follows: decreasing the emitter width excessively, decreases the volume of active layer which, consequently, decreases the number of generated carriers. On the other hand, increasing the emitter width much higher than the diffusion length of carriers, increases the number of lost carriers by recombination in the space outside the depletion layer. The same behavior happens for both values of emitter doping although the maximum efficiency for the lower doping is higher. The maximum efficiency is attained at an emitter width of 0.1 µm and doping concentration of 2×10^{19} cm^{-3}.

Table 4: Electrical performance parameters of various emitter thickness at two doping values: 2×10^{19} and 5×10^{19} cm^{-3}.

Thickness (μm)	**0.06**		**0.08**		**0.1**		**0.12**	
Doping (cm^{-3})	**2×10^{19}**	**5×10^{19}**	**2×10^{19}**	**5×10^{19}**	**2×10^{19}**	**5×10^{19}**	**2×10^{19}**	**5×10^{19}**
I_{sc} (nA)	6.89	6.887	6.89	6.89	6.9	6.89	6.90	6.89
V_{oc} (V)	0.579	0.576	0.583	0.578	0.583	0.579	0.576	0.577
***FF* (%)**	79.52	79.25	81.92	81.07	82.18	82.16	79.12	82.12
η_c (%)	14.18	14.05	14.71	14.44	14.77	14.66	14.07	14.6

C. Effect of the p^+ Base Width

In this subsection, the effect of variation of the p^+ base width, W_p, is introduced. The best value of W_p which gives the best performance is chosen such that the bulk recombination is minimized. The bulk recombination is controlled by the relation between W_p and L_n. When W_p is less than L_n, the light generated carriers reach the pn junction before they recombine. Thus, they are separated and collected. As a result, the performance of the *npn* structure enhanced. When W_p is equal to or greater than L_n, the light generated carriers start to recombine before reaching the sidewall pn junction. Thus, the *npn* structure performance is degraded. In the previous studies, L_n, W_p and τ_{n0} are chosen as a worst-case design when p^+ base doping is 10^{18} cm^{-3} [10]. L_n is assumed to be 12 μm; W_p is chosen to be 8 μm less than L_n to overcome bulk recombination and τ_{n0} is chosen to be 5 μsec.

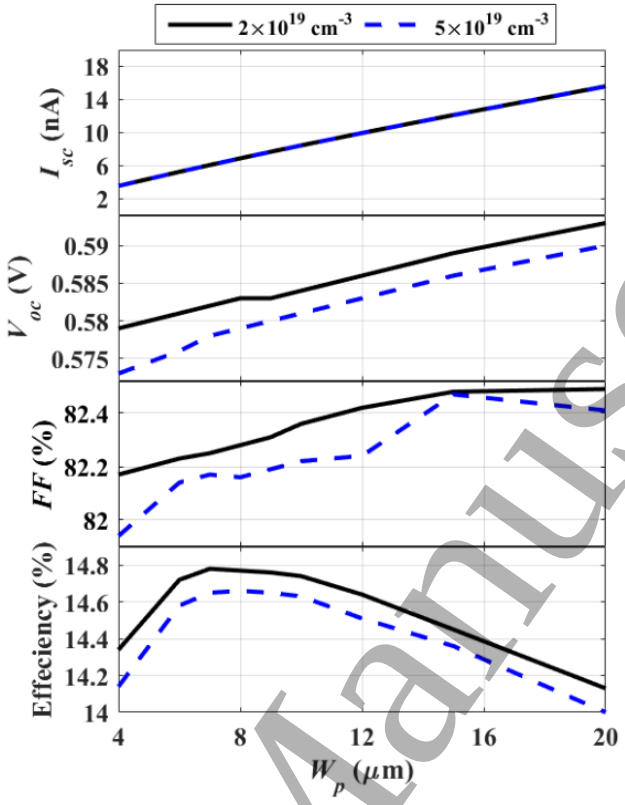

Figure 4. Solar cell parameters versus base width for two different values of emitter doping.

In this study, the doping of p^+ base is fixed to 10^{18} cm^{-3}. There are various values for W_p are going to be studied. The selected range of values for W_p is between 4 and 20 μm 12 (noting that L_n = 12 μm). When $W_p > L_n$, the performance of the *npn* structure is expected to be degraded. Figure 4 gives a clear comparison between the electrical performance parameters for the studied cases of the p^+ base width. For I_{sc}, it increases with increasing W_p due to the increasing of the exposed area to the input solar radiation spectrum. When W_p is less than L_n, the bulk recombination is neglected. Thus, all the light generated carriers reach the pn junction are separated and collected. When W_p equals to or exceeds L_n, the bulk recombination becomes effective. Regarding V_{oc}, as the reverse saturation current decreases with increasing W_p, thus V_{oc} increases. From the figure, it is obvious that, the best value for W_p is 7 μm for emitter doping of 2×10^{19} cm^{-3}. It gives the best efficiency for the *npn* structure. This result is expected. As the best W_p is expected to be less than L_n, where the bulk recombination is neglected.

A comparison between the *npn* structure optical performance is also carried out. Firstly, the quantum efficiencies for all cases are presented. Then, the spectral responses are illustrated. Figure

5(a) shows the quantum efficiency for the studied cases of the p^+ base width. It is obvious that the quantum efficiency increases with increasing W_p. This result is expected, as with increasing W_p, the exposed area for the input solar radiation spectrum increases and hence the rate of the generated carriers is increased. For low energy photons the quantum efficiency is lowered due to bulk recombination as $W_p > L_n$. Next, Figure 5(b) presents the spectral response for the studied cases of the p^+ base width. Based on the discussion of the *I–V* characteristics and electrical performance, the spectral response for four case studies is examined. As the spectral response is an indication for I_{sc}, thus it increases with increasing W_p as shown in figure 5(b).

D. Effect of Notch Depth

The carriers' collection area is proportional to the notch depth. So, the collected carriers, and hence, the output current is affected by the notch depth. As the notch depth increases, the collected current increases. This is observed from the current density distribution in Figure 6 for three different notch depths (75, 40 and 20 μm). Another important parameter affects the rate of the collected carriers which is the surface recombination, as the depth increases, the surface recombination increases which reduces the rate of increasing of the current as illustrated in Figure 7. A notch depth of greater than 50 μm is a suitable choice to achieve a considerable efficiency. Choosing lower notch depth is preferable for easier fabrication processes as this requires less aspect ratio.

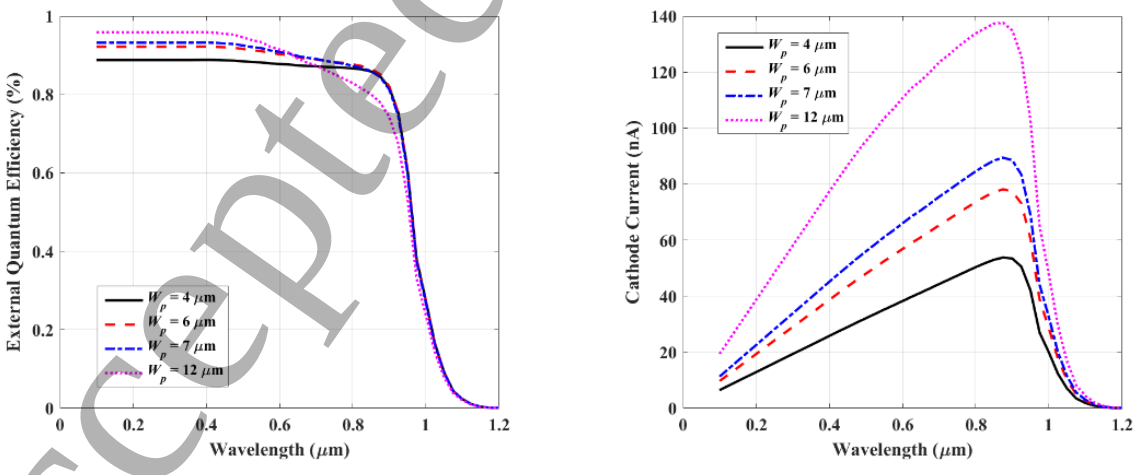

(a) (b)

Figure 5. Impact of the p^+ base width on (a) Quantum efficiency(b) Spectral response.

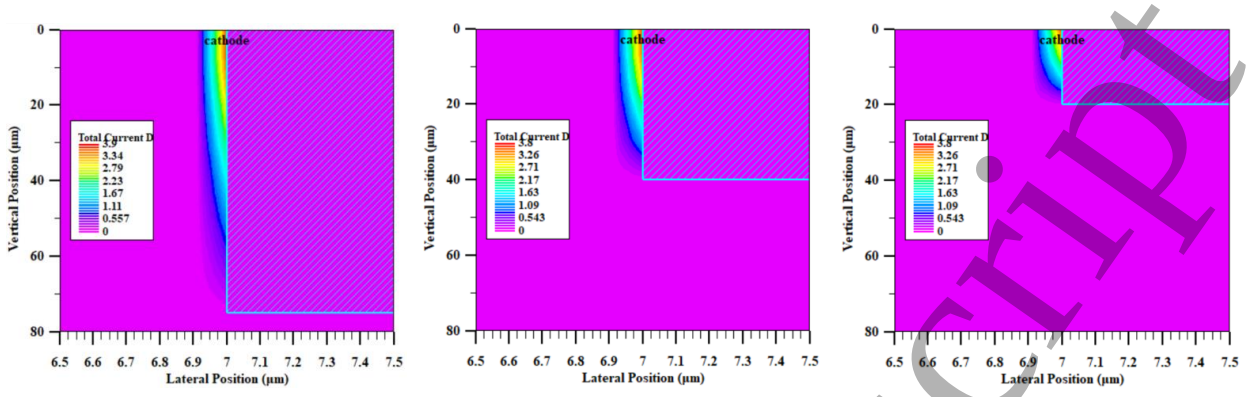

(a) (b) (c)

Figure 6. Electron Current density distribution for three different notch depths: (a) 75, (b) 40 and (c) 20 μm.

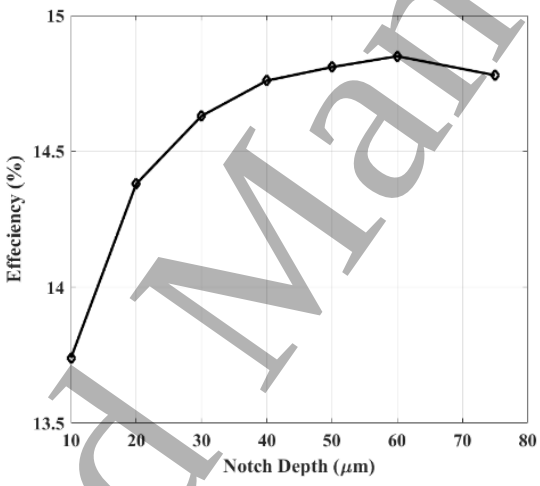

Figure 7. Impact of the Notch depth on the solar cell efficiency.

E. Effect of Back Surface

In this subsection, the effect of the *npn* structure back surface is presented. In the conventional planar solar cell [22], its back surface must be treated by the back-surface reflector. This is done by inserting a p^{++} layer at the cell back surface. This layer reduces the back-surface recombination in the conventional planar solar cells. Thus, it enhances both its dark and illumination characteristics. It is also important to investigate the effect of the back-surface treatment on the performance of the *npn* structure. Figure 8 shows the *npn* structure without and with the back-surface treatment.

Only the electrical performance parameters of the *npn* structure with and without p^{++} at its back surface are going to be compared. Table 5 contains the extracted electrical performance parameters for the *npn* structure without and with p^{++} layer on its back surface. From table 5, it is obvious that, I_{sc} has a very slight increase due to the effect of the p^{++} layer on the back surface of the *npn* structure. It means that it doesn't enhance the illumination characteristics of the *npn* structure. For V_{oc}, it is the same for the same reason. Additionally, the fill factor is increased by 0.9%. As a result, the *npn* structure conversion efficiency is enhanced by 0.1% because of the structure back surface treatment.

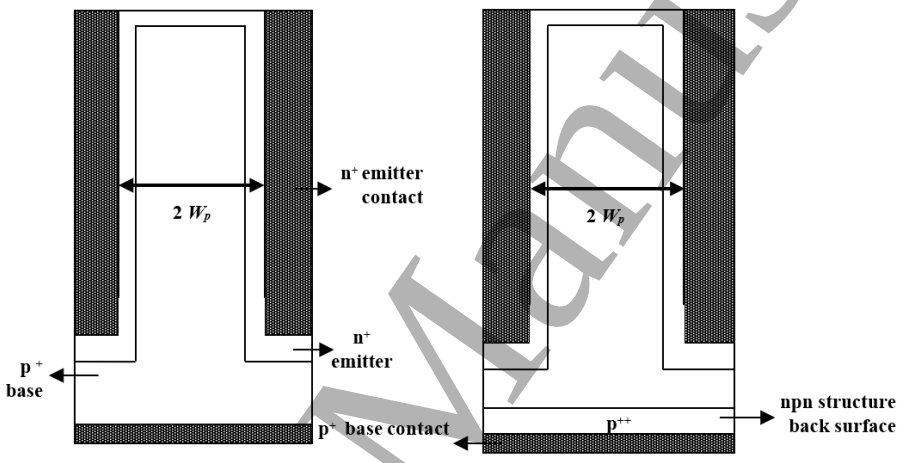

Figure 8. (a) *npn* structure (no p^{++} at back surface) (b) *npn* structure (p^{++} at back surface).

Table 5 Electrical performance parameters of the *npn* structure back surface.

	No p^{++} at back surface	**p^{++} at back surface**
I_{sc} (nA)	6.09	6.1
V_{oc} (V)	0.582	0.584
FF (%)	82.25	82.33
η_c (%)	14.78	14.87

Finally, the dark characteristic of the proposed structure (given $W_p = 7$ μm) is investigated in order to have an in-depth understanding of the recombination mechanisms occurring within the various device regions. From Figure 9, it can be observed that the proposed npn shows a two-diode

characteristic. A curve fit was used to estimate the parameters from the TCAD simulation data. In 0.1 V to 0.4 V regime, the exponential approximation of the ideality factor is 1.8. From 0.5 V to 0.6 V, the ideality factor is 1.0 like an ideal diode. Figure 10 shows the recombination rates within the device taking a horizontal cutline 5 μm below the upper surface. The figure illustartes the recombination rates within the emitter, depletion region and a part of the base. The electric field is also shown to identify the depletion region boundaries. It is evident from Figure 10(a) that the depletion recombination is much higher than the emitter recombination for low voltage (0.2 V); while, for a higher voltage (at V = 0.6 V) in Figure 11(b), the recombination rate within the emitter becomes higher than the depletion. This explains the values of the extracted ideality factor as higher values than 1 describes the recombination current, which is mainly due to recombination in the depletion region whereas the value of 1.0 describes the diffusion current due to the recombination in the emitter and base of the cell [26].

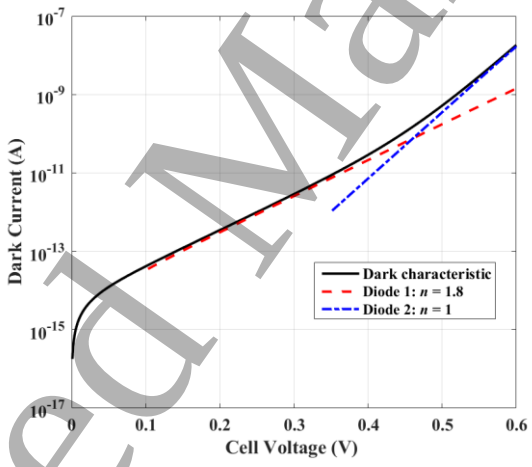

Figure 9 Dark IV characteristics for W_p = 7 μm showing the fit of two-diode model.

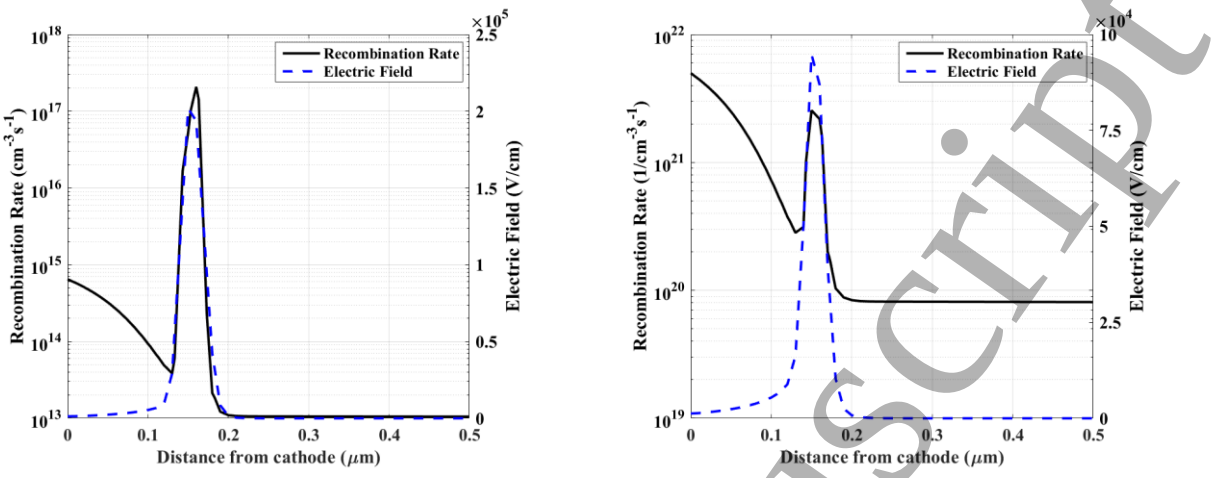

(a) (b)

Figure 10 Recombination rate and electric field at a horizontal cutline within the solar cell structure for forward bias dark characteristics (a) V = 0.2 V and (b) V = 0.6 V.

Moreover, the impact of the geometrical changes on the ideality factor is studied to explain the behavior of the cell according to the recombination mechanisms. Figure 11 shows the local ideality factor for three cases of base width W_p = 4, 7 and 20 µm. Similar behavior is observed for the three cases meaning that the recombination mechanisms do not depend on a high extent on the base width. A difference of the local ideality factor is observed for the 0.5-0.6 voltage regime which is responsible for the fill factor behavior observed in Figure 4. Although there is an enhancement in the ideality factor due to the increase in the base width, the efficiency is optimum for a certain width (which is W_p = 7 µm). This could be explained by noting that the short circuit current density of the optimized width is the highest amongst the other widths. The values of the short circuit current density are 39.7, 40.6 and 38 mA/cm^2 for W_p = 4, 7 and 20 µm, respectively.

It might be pointed out here that the proposed npn structure fabrication requires the same matured process flow of fabricating the conventional planar solar cell. The only additional step is to open the vertical notches by producing deep trenches. This additional uncostly fabrication step could be achieved by deep trench ion etching (DRIE) process which is easily capable in etching such deep trenches specially for an aspect ratio less than 1:75 as in our structure [27].

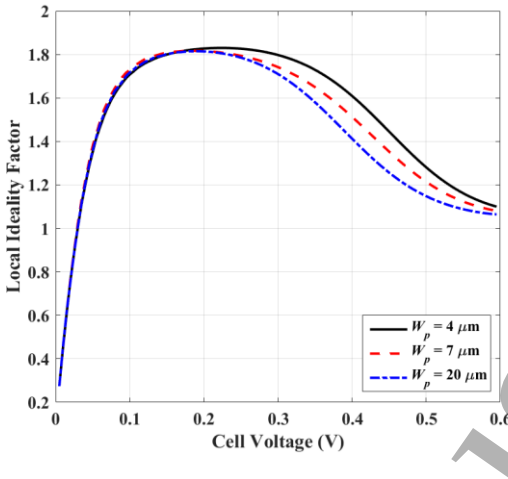

Figure 11 Local ideality factor vs. cell voltage for different values of base width.

4. Conclusion

In this paper, an approach has been used to avoid the need for high diffusion length that is required in conventional planar solar cells and so high-quality costly Si wafers. An npn structure geometry is utilized in which the direction of light absorption is decoupled from that of carrier collection. The performance of *npn* solar cell structure is enhanced by optimizing its geometrical and technological parameters. All simulations are carried out using SILVACO TCAD. The enhancement in conversion efficiency is achieved by the optimization of various parameters. Firstly, the top n^+ layer thickness and doping are adjusted to satisfy ultraviolet collection. The best thickness for the top n^+ layer is 0.1 μm and its best doping 2×10^{19} cm^{-3}. Then, the effect of the design of the *npn* structure sidewall n^+ emitter on its performance is studied. In addition, the effect of the variation of the p^+ base width on its performance is studied. Experimentally validated values of diffusion lengths and lifetimes are used. According to these values, the best base width is selected. As a result, the *npn* structure active area which exposed to the input solar radiation spectrum increases. Thus, overall performance of the *npn* structure is greatly enhanced. Due to the optimization of the *npn* structure W_p, its conversion efficiency is enhanced by 3.5%. Finally, the effect of the back-surface treatment on the *npn* structure is studied and the conversion efficiency is increased from about 14.8 to 14.9%. The *npn* structure is designed to satisfy an efficiency of about 15%, with low cost thin (80 μm), highly-doped (10^{18} cm^{-3}) silicon wafers. The enhancement of the structure performance is based on real fabrication considerations as the used life time and

diffusion length values are extracted from practical measurement of silicon wafers. As a future work, the optimized npn solar cell structure could be utilized in a flipped way. In this regard, the illumination performance of the structure will increase as the shadowing due to the structure notches is removed. Thus, it is expected to provide more enhancement to the structure performance.

References

[1] ITRPV, "International Technology Roadmap for Photovoltaic (ITRPV)," 2015.

[2] A. I. Hochbaum and P. Yang, "Semiconductor nanowires for energy conversion," *Chemical reviews,* vol. 110, pp. 527-546, 2009.

[3] M. A. Green*, et al.*, "Solar cell efficiency tables (version 46)," *Progress in Photovoltaics: Research and Applications,* vol. 23, pp. 805-812, 2015.

[4] D. L. Staebler and C. R. Wronski, "Reversible conductivity changes in discharge□produced amorphous Si," *Applied Physics Letters,* vol. 31, pp. 292-294, 1977.

[5] D. Amkreutz*, et al.*, "Silicon Thin-Film Solar Cells on Glass With Open-Circuit Voltages Above 620 mV Formed by Liquid-Phase Crystallization," *IEEE Journal of Photovoltaics,* vol. 4, pp. 1496-1501, 2014.

[6] C. W. Teplin*, et al.*, "Comparison of thin epitaxial film silicon photovoltaics fabricated on monocrystalline and polycrystalline seed layers on glass," *Progress in Photovoltaics: Research and Applications,* vol. 23, pp. 909-917, 2015.

[7] A. Goodrich*, et al.*, "A wafer-based monocrystalline silicon photovoltaics road map: Utilizing known technology improvement opportunities for further reductions in manufacturing costs," *Solar Energy Materials and Solar Cells,* vol. 114, pp. 110-135, 2013/07/01/ 2013.

[8] M. D. Kelzenberg*, et al.*, "Single-nanowire Si solar cells," in *2008 33rd IEEE Photovoltaic Specialists Conference*, 2008, pp. 1-6.

[9] M. C. Putnam*, et al.*, "Si microwire-array solar cells," *Energy & Environmental Science,* vol. 3, pp. 1037-1041, 2010.

[10] M. Salem*, et al.*, "Design and simulation of proposed low cost solar cell structures based on heavily doped silicon wafers," in *Photovoltaic Specialist Conference (PVSC), 2017 IEEE 44th*, 2017, pp. 1-5.

[11] *Athena*. Available: https://www.silvaco.com/products/tcad/process_simulation/athena/athena.html

[12] A. Zekry, "The dependence of diffusion length, lifetime and emitter Gummel-number on temperature and doping," *Archiv für Elektrotechnik,* vol. 75, pp. 147-154, 1992.

[13] O. Palais*, et al.*, "High resolution lifetime scan maps of silicon wafers," *Materials Science and Engineering: B,* vol. 71, pp. 47-50, 2000.

[14] A. Cuevas and D. Macdonald, "Measuring and interpreting the lifetime of silicon wafers," *Solar Energy,* vol. 76, pp. 255-262, 2004.

[15] J. Del Alamo*, et al.*, "Simultaneous measurement of hole lifetime, hole mobility and bandgap narrowing in heavily doped n-type silicon," in *Electron Devices Meeting, 1985 International*, 1985, pp. 290-293.

[16] J. A. del Alamo and R. M. Swanson, "Modelling of minority-carrier transport in heavily doped silicon emitters," *Solid-State Electronics,* vol. 30, pp. 1127-1136, 1987.

[17] *Atlas*. Available:

https://www.silvaco.com/products/tcad/device_simulation/atlas/atlas.html

[18] R. Santbergen and R. C. van Zolingen, "The absorption factor of crystalline silicon PV cells: A numerical and experimental study," *Solar Energy Materials and Solar Cells,* vol. 92, pp. 432-444, 2008.

[19] F. Toor*, et al.*, "17.1%-efficient multi-scale-textured black silicon solar cells without dielectric antireflection coating," in *Photovoltaic Specialists Conference (PVSC), 2011 37th IEEE*, 2011, pp. 000020-000024.

[20] M. A. Green and M. J. Keevers, "Optical properties of intrinsic silicon at 300 K," *Progress in Photovoltaics: Research and Applications,* vol. 3, pp. 189-192, 1995.

[21] J. H. Gibson, "UVB RADIATION, Definition and Characteristics," Natural Resource Ecology Laboratory, Colorado State University, 2018.

[22] A. Luque and S. Hegedus, *Handbook of photovoltaic science and engineering*: John Wiley & Sons, 2011.

[23] C. E. Small*, et al.*, "High-efficiency inverted dithienogermole–thienopyrrolodione-based polymer solar cells," *Nature Photonics,* vol. 6, p. 115, 2012.

[24] P. Kittidachachan*, et al.*, "An analysis of a 'dead layer' in the emitter of n/sup+/pp/sup+/solar cells," in *Photovoltaic Specialists Conference, 2005. Conference Record of the Thirty-first IEEE*, 2005, pp. 1103-1106.

[25] S. L. Upstone, "Ultraviolet/visible light absorption spectrophotometry in clinical chemistry," *Encyclopedia of Analytical Chemistry: Applications, Theory and Instrumentation,* 2006.

[26] A. Zekry, A. Shaker and M. Salem, "Solar Cells and Arrays: Principles, Analysis, and Design," *Advances in Renewable Energies and Power Technologies*, pp. 3-56, 2018.

[27] M. T. Ghoneim and M. M. Hussain, "Highly Manufacturable Deep (Sub□Millimeter) Etching Enabled High Aspect Ratio Complex Geometry Lego□Like Silicon Electronics," *Small*, 13(16), 1601801, 2017.